Published in final edited form as:
Ultrasound Med Biol. 2013 July ; 39(7): 1267–1276. doi:10.1016/j.ultrasmedbio.2013.01.023.

Enhanced intracellular delivery of a model drug using microbubbles produced by a microfluidic device

Adam J. Dixon[a], **Ali H. Dhanaliwala**[a], **Johnny L. Chen**[a], and **John A. Hossack**[a,*]
[a]Department of Biomedical Engineering, University of Virginia, Charlottesville, Virginia, USA

Abstract

Focal drug delivery to a vessel wall facilitated by intravascular ultrasound and microbubbles holds promise as a potential therapy for atherosclerosis. Conventional methods of microbubble administration result in rapid clearance from the blood stream and significant drug loss. To address these limitations, we evaluated whether drug delivery could be achieved with transiently stable microbubbles produced in real-time and in close proximity to the therapeutic site. Rat aortic smooth muscle cells were placed in a flow chamber designed to simulate physiological flow conditions. A flow-focusing microfluidic device (FFMD) produced 8 μm diameter monodisperse microbubbles within the flow chamber, and ultrasound was applied to enhance uptake of a surrogate drug (calcein). Acoustic pressures up to 300 kPa and flow rates up to 18 mL/s were investigated. FFMD generated microbubbles were stabilized with a polyethylene glycol-40 stearate shell and had either a perfluorobutane (PFB) or nitrogen gas core. The gas core composition affected stability, with PFB and nitrogen microbubbles exhibiting half-lives of 40.7 and 18.2 seconds, respectively. Calcein uptake was observed at lower acoustic pressures with nitrogen microbubbles (100 kPa) than with PFB microbubbles (200 kPa) ($p < 0.05$, $n \geq 3$). In addition, delivery was observed at all flow rates, with maximal delivery (> 70% of cells) occurring at a flow rate of 9 mL/s. These results demonstrate the potential of transiently stable microbubbles produced in real-time and in close proximity to the intended therapeutic site for enhancing localized drug delivery.

Keywords

Flow focusing microfluidic device; monodisperse microbubbles; ultrasound mediated drug delivery; sonoporation

Introduction

Ultrasound enhanced drug and gene delivery has been investigated extensively in recent years. Early work by Fechheimer et al. (1987) demonstrated increased uptake of plasmid DNA at 20 kHz. Bao et al. (1997) extended this work by adding microbubbles and insonating at 2.25 MHz to enhance uptake of a luciferase plasmid. Since then, numerous reports studying the effect of various ultrasound (e.g. frequency, pressure, duty cycle) and microbubble (e.g. shell composition, microbubble concentration) parameters on drug and

*Corresponding Author: John A Hossack, PO Box 800759 Charlottesville, VA 22908; jh7fj@virginia.edu; Phone, 434-243-5866.

gene delivery have been published (Guzmán et al., 2001; Larina et al., 2005; Mehier-Humbert et al., 2005; Hallow et al., 2006; Hassan et al., 2010; Phillips et al., 2011b).

Although there is increasing interest in ultrasound-mediated drug and gene delivery to large blood vessels for the treatment of atherosclerosis (Phillips et al., 2010, 2011a), the effects of blood flow on ultrasound-mediated delivery have not been extensively studied. The majority of parameter optimization has been conducted *in vitro* under static conditions, but it is known that blood flow patterns alter local drug and microbubble concentrations within the vessel (Patil et al., 2009). Static conditions fail to provide a means to study the effects of blood flow rate on drug delivery, but adding fluid flow to *in vitro* models of drug delivery may allow for better translation of optimized ultrasound parameters to *in vivo* settings.

Enhanced delivery requires precise control over both ultrasound and microbubble parameters. While ultrasound parameters are easily controlled and models exist for the propagation of acoustic waves through tissue (Jensen, 1991; Zemp et al., 2003), the properties of microbubbles are less predictable. First, the majority of current microbubble production techniques utilize agitation methods (Klibanov, 2002), which generate microbubbles with a wide range of diameters (i.e. polydisperse) (Stride and Edirisinghe, 2009). Populations of polydisperse microbubbles are characterized by a distribution of resonance frequencies related to the size distribution of the microbubble population. The range of resonance frequencies results in reduced imaging sensitivity when compared to imaging monodisperse populations (Kaya et al., 2010; Streeter et al., 2010) and may affect drug delivery efficacy (Choi et al., 2010). Additional improvements in imaging sensitivity with monodisperse microbubble populations may be achieved if the microbubble resonance frequency is matched to the peak frequency of the imaging pulse (Talu et al., 2007). Second, a large percentage of microbubbles are lost following intravenous administration and circulation (Butler and Hills, 1979; Lim et al., 2004; Iijima et al., 2006; Talu et al., 2008b), resulting in poor control of microbubble and drug concentrations at the therapeutic target site. Finally, while the acoustic properties of single microbubbles have been experimentally observed and modeled (Church, 1995; Morgan et al., 2000; de Jong et al., 2002; Marmottant et al., 2005; Patil et al., 2010), the interactions between clouds of oscillating microbubbles and the impact of these interactions on the processes that govern drug delivery remain unclear.

To overcome some of these limitations, we propose the production of microbubbles from a catheter located within the vasculature – i.e. *in situ* microbubble production – to enable local administration of a well-controlled number of monodisperse microbubbles and a controlled total drug dose. Flow-focusing microfluidic devices (FFMDs) (Gordillo et al., 2004; Garstecki et al., 2004; Hettiarachchi et al., 2007; Castro-Hernández et al., 2011) are ideal for this application, as they have a small footprint (Dhanaliwala et al., 2012) and can produce microbubbles in real-time in a continuous manner. FFMDs produce microbubbles by compressing a central gas column with two liquid streams containing the microbubble shell material (Tan et al., 2006). In addition, FFMDs produce monodisperse microbubbles (Hettiarachchi et al., 2007; Stride and Edirisinghe, 2009), and microbubble diameter can be "tuned" to the requirements of specific applications by adjusting the gas and liquid input parameters. Producing microbubbles directly within the vasculature significantly reduces the number of microbubbles needed for contrast enhancement or drug delivery, as losses due to storage, administration, and circulation are eliminated. Thus, microbubble production rates currently achieved by FFMDs, ranging from 10^3 to 10^6 microbubbles per second (Stride and Edirisinghe, 2009), may be sufficient to enhance drug delivery.

Another advantage of *in situ* microbubble production is the ability to investigate unconventional microbubble formulations. Microbubbles produced in the vasculature at the

therapeutic target site do not require long circulation lifetimes. Unstable formulations (e.g. microbubbles with N_2, CO_2, or O_2 gas cores and a mild surfactant shell) that would otherwise quickly dissolve if administered systemically (Kabalnov et al., 1998; Park et al., 2010), could be insonated immediately following production. Furthermore, larger microbubbles, which provide increased acoustic contrast (Dalla Palma and Bertolotto, 1999; Gorce et al., 2000) and improved sonoporation (Deng et al., 2004; Fan et al., 2012), may be viable since quick dissolution reduces the embolic risk.

In this paper, we demonstrate the feasibility of *in situ* produced microbubbles for drug delivery *in vitro*. To better simulate *in vivo* flow conditions, we developed a flow chamber that enables the study of ultrasound-mediated drug delivery to a cell monolayer under physiological flow conditions. A flow-focusing microfluidic device was used to produce microbubbles in real-time, and the effect of microbubble composition and flow rate on model drug delivery to cells was assessed by fluorescence microscopy.

Materials and Methods

FFMD Fabrication

Flow-focusing microfluidic devices were fabricated as described previously (Dhanaliwala et al., 2012). Briefly, a custom SU-8 mold was manufactured by photomicrolithography. Devices were cast in polydimethylsiloxane (PDMS) (Sylgard 184, Dow Corning Corp., Midland, MI) and bound to a clean PDMS substrate using oxygen plasma. The final device had a channel height of 25 μm and a nozzle width of 8 μm, while the liquid and gas channels were 50 and 30 μm wide, respectively. The overall dimension of the device used in this study was 10 × 4 × 8 mm. Water was introduced into the microchannels immediately after binding to maintain hydrophilicity of the channels. Devices were stored in deionized water and were used within five days.

Microbubble Characterization

The liquid phase consisted of 15 mg/mL polyethylene glycol-40-stearate (PEG40S) dissolved in a solution of 10% glycerol, 10% propylene glycol, and 80% phosphate buffered saline with magnesium and calcium (v/v) (GPS). All chemicals were purchased from Sigma-Aldrich (St. Louis, MO). The PEG40S-GPS solution was sonicated to at least 60 °C with a tip sonicator (XL2020, Misonix, Farmingdale, NY) using a half-inch probe (40% power, 7 min) and sterile filtered (0.45 μm nylon flter, Fisher Scientific Waltham, MA) prior to use. The gas phase was either nitrogen (GTS Welco, Richmond, VA) or perfluorobutane (PFB) (Synquest, Alachua, FL). PTFE microbore tubing (Cole Parmer, Vernon Hills, IL) was used to interconnect the liquid and gas phases with the microfluidic device. The liquid flow rate was controlled via a syringe pump (PHD2000 Harvard Apparatus, Holliston, MA) and the gas pressure was controlled via a regulator and a digital manometer.

A high speed camera (SIMD24, Specialised Imaging, Tring, United Kingdom) connected to an inverted microscope was used to characterize microbubble production as described previously (Dhanaliwala et al., 2012). The gas pressure and liquid flow rate that provided the smallest stable microbubbles were used for the calcein delivery experiments. Stable microbubble production was defined as gas and liquid parameters that did not result in microbubble fusion within the microfluidic device.

To determine microbubble stability, a FFMD producing microbubbles was placed in 100 mL of air-saturated saline for 5 seconds at 25 °C. The FFMD was removed and the solution was then analyzed using a Coulter Particle Counter (Z2 particle analyzer, Beckman Coulter, Brea, CA). The solution was stirred continuously while measurements were taken every 30 seconds for 2 minutes.

Cell Culture and Calcein Delivery

Primary rat aortic smooth muscle cells were plated on Thermanox cover-slips (Nunc, Rochester, NY) at a density of 5×10^3 cells/cm^2 and incubated at 37 °C in a 5 % CO_2 environment. The smooth muscle cells were cultured in growth media (DMEM/F12 plus 10 % fetal bovine serum, Gibco, Grand Island, NY) and were allowed to reach 100 % confluency prior to experimentation. Smooth muscle cells were used in this study as they are often the target of antiproliferative therapeutics to reduce restenosis following balloon angioplasty procedures (Phillips et al., 2011a,b).

A custom flow chamber (Fig 1A) designed to mimic laminar arterial flow was constructed from cast acrylic. The chamber was 0.2 cm high by 2.4 cm wide by 18 cm long and contained an acoustic window (50 μm thick mylar, McMaster-Carr, Atlanta, GA) half-way down its length. The dimensions were selected to ensure laminar flow within the chamber and to enable analytical determination of the shear stress experienced by the cells, which is given by: $\tau_w = \frac{6\mu Q}{bh^2}$, with μ = fluid viscosity, Q = flow rate, b = width of chamber, and h = height of chamber (Bacabac et al., 2005). A Thermanox coverslip containing confluent smooth muscle cells was placed within the acoustic window, and the flow chamber was submerged in 155mM phosphate buffered saline with calcium and magnesium (PBS +/+) (Gibco, Grand Island, NY) at 37 °C. Flow was established by pulling PBS +/+ through the flow chamber using a peristaltic pump (Wheaton Science Products, Millville, NJ). Microbubbles were introduced by placing a pre-characterized FFMD within the channel.

Calcein (Sigma-Aldrich, St. Louis, MO), a fluorophore that cannot pass through intact cell membranes, was used as a model therapeutic since only living cells that are permeabilized by ultrasound and microbubbles internalize calcein and fluoresce (Guzmán et al., 2001). A concentrated calcein solution was administered from a separate tube affixed to the FFMD to achieve a final concentration of 0.05 mg/ml within the flow chamber for each flow rate.

Ultrasound was applied by a focused, 1 inch diameter, 500 kHz single-element ultrasound transducer (V301 Olympus Panametrics, Waltham, MA) positioned at half the focal distance above the acoustic window. The transducer was driven by a 30 cycle, 500 kHz sinusoid at a pulse repetition frequency (PRF) of 100 Hz. The waveform was supplied by an arbitrary waveform generator (AWG3022B, Tektronix, Beaverton, OR) and amplified by a 60 dB RF power amplifier (A-500 ENI, Rochester, NY). Acoustic pressures were confirmed using a calibrated PVDF hydrophone (GL-0200, Onda Corp., Sunnyvale, CA). 500 kHz was selected as the ultrasound frequency to match the resonance of 8–10 μm diameter air-filled microbubbles (de Jong et al., 2002).

The cells were insonated under flow with microbubbles and calcein for a total of 2 minutes. The ultrasound and FFMD were then removed and the cells were incubated within the flow chamber under flow for an additional 2 minutes to allow cell membranes to completely reseal (Deng et al., 2004). The Thermanox membranes were removed, stained with 25 μg/ml propidium iodide (PI) (MP Biomedicals, Santa Ana, CA), a marker of cell death, and then imaged using fluorescence microscopy.

The effects of flow rate, acoustic pressure, and microbubble gas composition on intracellular delivery were investigated. At least three trials were conducted for each permutation of microbubble gas (nitrogen, PFB), chamber flow rate (2, 9, and 18 ml/s), and peak negative pressure (PNP) (0, 100, 200, 300 kPa).

Statistical Analysis

For each trial, four images of each membrane were acquired, and the number of cells that internalized calcein and the number of nuclei stained with PI in each image were counted. Since ultrasound can cause cells to dislodge from a membrane *in vitro* (Liu et al., 2012), percentages were calculated using the total number of cells prior to insonation. The average difference in total number of cells between four Thermanox membranes at 100 % confluency was less than 5 % and was therefore assumed to be equal for all subsequent membranes. Percent delivery was calculated as the total number of cells that internalized calcein divided by the total number of cells on the membrane prior to insonation. Percent death was calculated as the sum of PI positive and dislodged cells divided by the total number of cells prior to insonation. In all cases, Students *t*-tests were used to determine the statistical significance between experimental groups. A *p*-value of less than 0.05 was considered to be significant.

Results

Microbubble Characterization

Microbubbles were produced using a flow focusing microfluidic device at liquid flow rates between 40 and 76 μl/min and gas pressures between 48.3 and 55.2 kPa. Within this parameter range, stable microbubbles with diameters between 8 – 17 μm were produced at rates between $0.1–0.5\times10^6$ microbubbles/s. Increasing gas pressure or decreasing flow rate caused microbubble diameter to increase and production rate to decrease (Fig 1B–C). In addition, for a given diameter, microbubbles with a PFB gas core had a higher production rate as compared to microbubbles with a nitrogen gas core. The addition of calcein (10 mg/ml) directly to the liquid phase did not affect microbubble production (Fig 2A). All microbubbles were monodisperse at the device nozzle with a polydispersity index (standard deviation/mean) less than 6 % (Fig 2B). In addition, both PFB and nitrogen microbubbles remained monodisperse immediately after exiting the FFMD (Fig 2C–D).

Microbubble Stability

Microbubble size distribution and stability were observed to be dependent on the composition of the gas core ($n = 3$). For both gasses, the FFMD was calibrated to produce 8 μm diameter microbubbles. At the initial measurement, PFB microbubbles had already grown to an average diameter of greater than 10 μm but progressively shrank over time (Fig 3A). The number of PFB microbubbles present versus time was fitted to an exponential decay model ($R^2 = 0.95$), and the half-life was calculated to be 40.7 seconds (Fig 3A inset). Nitrogen microbubbles did not significantly expand when introduced to the air-saturated saline, and their half-life ($R^2 = 0.97$) was 18.2 seconds. For both gases, no microbubbles larger than 25 μm were detected by the Coulter Particle Counter. This result was also confirmed by observing microbubble populations via light microscopy. After 120 seconds, fewer than 1 % of the initial population of microbubbles were detected above the 5 μm lower threshold of the analyzer.

Drug Delivery – Flow Rate

The flow rates used in this study resulted in wall shear stresses consistent with cited values for arterial shear stress *in vivo* (1 – 15 dyne/cm^2) (Bacabac et al., 2005) and did not cause cell dislodgement. In addition, no calcein delivery was observed when either ultrasound or microbubbles were applied alone. Microbubble diameter and production rate were held constant at 10 μm and 300,000 microbubbles per second, respectively. Acoustic peak negative pressure was held constant at 300 kPa. Calcein delivery was observed at all flow rates (Fig 4A–C), with maximal delivery occurring at a flow rate of 9 mL/s and maximum

cell death at 2 mL/s (Fig 5). Approximately 31 % of cells were dislodged from the membranes at 2 mL/s, compared to 8 % and 6 % at 9 and 18 mL/s, respectively.

Drug Delivery – Pressure

Microbubble diameter and production rate were held constant at 10 μm and 300,000 microbubbles per second, respectively, while flow rate was held constant at 9 mL/s. The acoustic pressure required to enable calcein delivery was observed to depend on the composition of the microbubble gas core. For PFB microbubbles, delivery was only seen at peak negative pressures above 200 kPa (Fig 4D–F, Fig 6A). Minimal delivery and cell death was observed at pressures less than 200 kPa. For nitrogen microbubbles, delivery was observed at peak negative pressures above 100 kPa, and no significant differences in delivery or death were observed between pressures of 100 kPa and 300 kPa. (Fig 4G–I, Fig 6B).

The following controls were performed in the calcein delivery studies: (1) calcein delivery at 18 ml/s flow but without microbubbles or ultrasound, (2) calcein delivery without flow, without microbubbles, but with 300 kPa PNP ultrasound, and (3) calcein delivery without flow, without ultrasound, but with FFMD generated microbubbles. In addition, calcein delivery was measured when calcein alone or calcein with a PEG40S solution at the same concentration used to make the microbubbles was flowed past the cells. In all cases, negligible calcein delivery was observed.

Discussion

FFMD and Microbubble Characterization

Microfluidic device blockage caused by debris is a frequent problem in microfluidic device technology. Blockage in our device resulted primarily from contamination during the fabrication process and was not observed once a device began producing microbubbles. Robust device operation can be attributed to the incorporation of filters in the gas and liquid lines that trap contaminants introduced by the gas and liquid streams. These filters have previously been shown to enable stable microbubble production even when up to 90 % of the filters are blocked by contaminants (Wang et al., 2013).

Microbubble lifetimes and diameter fluctuations were evaluated in a continuously stirred, air-saturated media in order to more closely approximate the nitrogen saturated environment of blood found *in vivo* (Hall, 2010). PFB and nitrogen microbubbles maintained their monodispersity immediately following ejection from the FFMD and did not fuse form larger microbubbles (Fig 2C–D). Measurements recorded by the Coulter Particle Counter indicated that PFB microbubbles initially expanded, presumably due to an influx of air from the air-saturated medium (Talu et al., 2008a), and exhibited a longer half-life due to the initial volume expansion and low diffusivity of PFB (Fig 3A). The average diameter of nitrogen microbubbles, which were produced with 99.9 % nitrogen gas, expanded slightly following production but gradually decreased as the gas diffused out of the microbubble shell (Fig 3B). In comparison, lipid-shelled microbubbles with PFB cores produced via agitation exhibited no change in diameter or number over a 15 minute observation period (data not shown). Although these microbubble stability experiments were performed at 25 °C, the findings are consistent with reports of *in vivo* microbubble dissolution in the presence of large partial pressure gradients between the microbubble core and circulating blood, suggesting that microbubble coalescence with ambient gases is of low risk (Wible et al., 1996).

Drug Delivery and Flow Rate

Since FFMD microbubble production rates were held constant, flow rate dictated local microbubble concentration within the flow chamber (i.e. higher flow rates yielded lower microbubble concentrations). Thus, the observed peak in calcein delivery as a function of flow rate (Fig 5) may have been a consequence of optimized local microbubble concentration that occurred at 9 ml/s rather than a direct effect of the flow rate. At the lowest flow rate, microbubbles were visually confirmed to be highly concentrated. High concentrations of microbubbles increase cell dislodgement and death (Liu et al., 2012) (Fig 4A) and attenuate ultrasound, decreasing delivery efficiency as observed in our trials (Fig 5). At the highest flow rate, microbubbles were probably below the optimal microbubble-to-cell ratio, resulting in reduced calcein delivery (Fig 5). These observations support the hypothesis that microbubble parameters, including diameter and production rate, can be tuned to optimize sonoporation and delivery based upon local vascular conditions (Fan et al., 2012).

A similar flow-rate dependent effect may alter local drug concentrations if the drug is administered directly from the liquid phase of the FFMD. FFMD gas and liquid flow rates were adjusted to select optimal microbubble parameters. If the drug was present in the FFMD liquid phase, then adjusting the flow rate to change microbubble diameter or production rate would also alter the dispensation of the drug. To control for this effect, calcein was administered via a separate tube attached to the FFMD. The calcein concentration was held constant within the flow chamber (0.05 mg/ml) by adjusting the calcein dispensation rate according to changes in the channel flow rate. However, the presence of calcein in the liquid phase did not disrupt microbubble formation within the FFMD (Fig 2A), indicating that calcein, or another drug of choice that is either soluble in the microbubble shell or liquid solvent phase, could be incorporated directly within the FFMD.

Drug Delivery, Pressure, and Microbubble Composition

When insonated, both PFB and nitrogen microbubbles enhanced cellular uptake of calcein (Fig 6A–B). Furthermore, no significant differences in percent delivery or percent death were observed between either PFB or nitrogen microbubbles at acoustic pressures that enabled delivery. However, nitrogen microbubbles achieved delivery at a lower acoustic pressure threshold than PFB microbubbles. Additional testing is required to elucidate the mechanisms behind this observation, but one possibility is that the PFB microbubbles required more acoustic energy to cause sonoporation due to their increased stability and size. Microbubble resonance frequency effects may also play a role. PFB and nitrogen microbubbles were of equal size at the FFMD nozzle, and their resonance frequencies were well-matched immediately following production (de Jong et al., 2002). The increase in average PFB microbubble diameter that was observed upon exposure to air-saturated saline shifted the resonance frequency of the PFB microbubbles relative to the resonance frequency of the nitrogen microbubbles. This relative shift in resonance frequency may have contributed to the difference in sonoporation observed between the two microbubble formulations.

Significance of the Study

Recent work by Fan et al. (2012) suggests that membrane pore sizes produced by sonoporation increase with increasing microbubble diameter. Large, stable microbubbles produced via agitation techniques exhibit relatively long circulation lifetimes, which precludes their use *in vivo* due to embolic risk (Klibanov, 2002). The *in situ* production paradigm demonstrated here enabled the first evaluation of large, transiently stable microbubbles for drug delivery applications. Our results indicate that upwards of 70 % of

cells internalized calcein as a result of enhanced delivery using ultrasound and microbubbles at flow velocities and shear stresses comparable to those found *in vivo* (Ku, 1997; Bacabac et al., 2005). This level of enhanced delivery is significantly higher than what has been observed in other *in vitro* studies (Liu et al., 2012), most of which were performed under static conditions and used considerably smaller (diameter less than 4 μm) microbubbles.

Microbubble production rates suitable for drug delivery in our *in vitro* flow chamber were achieved by modifying the shell material from a lipid ($\mathcal{O}(10^3 - 10^4)$) to a mild surfactant ($\mathcal{O}(10^4 - 10^6)$). Although high production rates using a mild surfactant shell material have been demonstrated previously, the resulting microbubbles were never tested for functionality or stability in well-mixed, air-saturated environments (Hettiarachchi et al., 2007). While the transiently stable microbubbles used in this work would not be suitable for systemic administration, the *in situ* production paradigm allows the microbubbles to reach their target and be insonated before dissolution. Further testing is required to determine if these transiently stable microbubbles are suitable for *in vivo* applications, however, microbubbles produced by agitation techniques commonly achieve lower *in vitro* drug-delivery rates (Liu et al., 2012) and have been shown to be effective *in vivo* (Phillips et al., 2010, 2011a,b).

While the FFMD employed in these experiments was large compared to the vasculature, similar microfluidic devices have been produced by our group that possess dimensions appropriate for *in vivo* intravascular applications (Dhanaliwala et al., 2012). With minor modifications, this small microfluidic device could be incorporated into existing 9F catheters for imaging and therapeutic applications in the abdominal aorta, inferior vena cava, and aorta. Furthermore, advances in microfluidic device fabrication (Eddings et al., 2008; Dhanaliwala et al., 2012) and the use of new materials other than PDMS (Li et al., 2011; Bragheri et al., 2012) may enable the production of devices with even smaller dimensions for use in coronary applications.

We envision that this technology will complement existing catheter-based cardiovascular interventions, such as balloon angioplasty and stent placement, abdominal aortic aneurysm stent grafting, or heart valve replacement. The microbubbles may be used to delineate the borders of a plaque or aneurysm using IVUS imaging (Frijlink et al., 2006), guide stent deployment, or deliver a post-procedure therapy that cannot be administered systemically (Phillips et al., 2011a,b). Furthermore, unlike intravenous injection of stable microbubbles, which only persist in the circulation for a short period of time and have a limited therapeutic window (Ferrara et al., 2007), this technology may provide enhanced imaging contrast (Dhanaliwala et al., 2012) and therapeutic efficacy for the entire duration of a procedure by producing microbubbles in real-time and on-demand. As a result, this technology may provide significant benefits in terms of real-time guidance, dose reduction, and improved drug delivery to vascular targets without any disadvantages beyond those already associated with current catheter-based interventions.

Conclusions

We report the first attempt to enhance model drug delivery to cells using microbubbles produced *in situ*. By taking advantage of the small footprint and on-demand production capabilities of flow-focusing microfluidic devices, we produced microbubbles in real-time and in close proximity to the therapeutic target. *In situ* production capabilities removes the stability requirement for microbubbles and enables the investigation of unconventional, unstable, and larger diameter microbubbles for both contrast enhancement and drug delivery. In addition, *in situ* microbubble production allows intravascular co-injection of therapeutics and microbubbles, thus no longer limiting the selection of drugs to only those that can be attached onto or dissolved into the microbubble shell. Finally, by simulating *in*

vivo flow *in vitro*, we were able to investigate how variations in physiological flow rates *in vivo* might impact drug delivery efficacy.

Acknowledgments

This work is funded in part by National Institutes of Health grant NHLBI R01 HL090700 to ALK, JAH. The high speed camera was funded by a shared instrumentation grant S10 RR025594 to JAH. AJD is supported by a NSF Graduate Research Fellowship and AHD is supported by an American Heart Association Graduate Fellowship. The content is solely the responsibility of the authors and does not necessarily represent the official views of the NIH or AHA. The authors would like to thank Dr. Alexander Klibanov for helpful advice and Brian Shin for help with image analysis.

References

Bacabac RG, Smit TH, Cowin SC, Van Loon JJWA, Nieuwstadt FTM, Heethaar R, Klein-Nulend J. Dynamic shear stress in parallel-plate flow chambers. Journal of Biomechanics. 2005; 38:159–167. [PubMed: 15519352]

Bao S, Thrall BD, Miller DL. Transfection of a reporter plasmid into cultured cells by sonoporation in vitro. Ultrasound in Medicine & Biology. 1997; 23:953–959. [PubMed: 9300999]

Bragheri F, Minzioni P, Martinez Vazquez R, Bellini N, Paiè P, Mondello C, Ramponi R, Cristiani I, Osellame R. Optofluidic integrated cell sorter fabricated by femtosecond lasers. Lab on a chip. 2012; 1219:3779–84. [PubMed: 22868483]

Butler BD, Hills BA. The lung as a filter for microbubbles. Journal of Applied Physiology. 1979; 47:537–543. [PubMed: 533747]

Castro-Hernández E, van Hoeve W, Lohse D, Gordillo JM. Microbubble generation in a co-flow device operated in a new regime. Lab on a Chip. 2011; 11:2023–2029. [PubMed: 21431188]

Choi JJ, Feshitan JA, Baseri B, Wang S, Tung YS, Borden MA, Konofagou EE. Microbubble-size dependence of focused ultrasound-induced blood-brain barrier opening in mice in vivo. IEEE Transactions on Biomedical Engineering. 2010; 57:145–154. [PubMed: 19846365]

Church CC. The effects of an elastic solid surface layer on the radial pulsations of gas bubbles. The Journal of the Acoustical Society of America. 1995; 97:1510–1521.

Dalla Palma L, Bertolotto M. Introduction to ultrasound contrast agents: physics overview. European Radiology. 1999; 9 (Suppl 3):S338–342. [PubMed: 10602924]

de Jong, N.; Bouakaz, A.; Frinking, P. Echocardiography. Vol. 19. Mount Kisco; N.Y: 2002. Basic acoustic properties of microbubbles; p. 229-240.

Deng CX, Sieling F, Pan H, Cui J. Ultrasound-induced cell membrane porosity. Ultrasound in Medicine & Biology. 2004; 30:519–526. [PubMed: 15121254]

Dhanaliwala A, Chen J, Wang S, Hossack J. Liquid flooded flow-focusing microfluidic device for in situ generation of monodisperse microbubbles. Microfluidics and Nanofluidics. 2012:1–11.

Eddings MA, Johnson MA, Gale BK. Determining the optimal PDMSPDMS bonding technique for microfluidic devices. Journal of Micromechanics and Microengineering. 2008; 186:067001.

Fan Z, Liu H, Mayer M, Deng CX. Spatiotemporally controlled single cell sonoporation. Proceedings of the National Academy of Sciences. 2012; 109:16486–16491.

Fechheimer M, Boylan JF, Parker S, Sisken JE, Patel GL, Zimmer SG. Transfection of mammalian cells with plasmid DNA by scrape loading and sonication loading. Proceedings of the National Academy of Sciences. 1987; 84:8463–8467.

Ferrara KW, Pollard R, Borden M. Ultrasound microbubble contrast agents: fundamentals and application to gene and drug delivery. Annual review of biomedical engineering. 2007; 9:415–47.

Frijlink ME, Goertz DE, Vos HJ, Tesselaar E, Blacquière G, Gisolf A, Krams R, van der Steen AFW. Harmonic intravascular ultrasound imaging with a dual-frequency catheter. Ultrasound in Medicine & Biology. 2006; 3211:1649–54. [PubMed: 17112951]

Garstecki P, Gitlin I, DiLuzio W, Whitesides GM, Kumacheva E, Stone HA. Formation of monodisperse bubbles in a microfluidic flow-focusing device. Applied Physics Letters. 2004; 85:2649–2651.

Gorce JM, Arditi M, Schneider M. Influence of bubble size distribution on the echogenicity of ultrasound contrast agents: a study of SonoVue. Investigative Radiology. 2000; 35:661–671. [PubMed: 11110302]

Gordillo JM, Cheng Z, Gañán Calvo AM, Marquez M, Weitz DA. A new device for the generation of microbubbles. Physics of Fluids. 2004; 16:2828.

Guzmán HR, Nguyen DX, Khan S, Prausnitz MR. Ultrasound-mediated disruption of cell membranes. II. heterogeneous effects on cells. Journal of the Acoustical Society of America. 2001; 110:597–606. [PubMed: 11508985]

Hall, JE. Elsevier Health Sciences. 2010. Guyton and Hall Textbook of Medical Physiology: Enhanced E-book.

Hallow DM, Mahajan AD, McCutchen TE, Prausnitz MR. Measurement and correlation of acoustic cavitation with cellular bioeffects. Ultrasound in Medicine & Biology. 2006; 32:1111–1122. [PubMed: 16829325]

Hassan MA, Buldakov MA, Ogawa R, Zhao QL, Furusawa Y, Kudo N, Kondo T, Riesz P. Modulation control over ultrasound-mediated gene delivery: evaluating the importance of standing waves. Journal of controlled release: official journal of the Controlled Release Society. 2010; 141:70–76. [PubMed: 19720097]

Hettiarachchi K, Talu E, Longo ML, Dayton PA, Lee AP. On-chip generation of microbubbles as a practical technology for manufacturing contrast agents for ultrasonic imaging. Lab on a Chip. 2007; 7:463–468. [PubMed: 17389962]

Iijima H, Moriyasu F, Miyahara T, Yanagisawa K. Ultrasound contrast agent, levovist microbubbles are phagocytosed by kupffer cells-in vitro and in vivo studies. Hepatology Research: The Official Journal of the Japan Society of Hepatology. 2006; 35:235–237. [PubMed: 16831566]

Jensen JA. A model for the propagation and scattering of ultrasound in tissue. The Journal of the Acoustical Society of America. 1991; 89:182–190. [PubMed: 2002167]

Kabalnov A, Klein D, Pelura T, Schutt E, Weers J. Dissolution of multicomponent microbubbles in the bloodstream: 1. theory. Ultrasound in Medicine & Biology. 1998; 24:739–749. [PubMed: 9695277]

Kaya M, Feingold S, Hettiarachchi K, Lee AP, Dayton PA. Acoustic responses of monodisperse lipid-encapsulated microbubble contrast agents produced by flow focusing. Bubble Science Engineering and Technology. 2010; 2:33–40. [PubMed: 21475641]

Klibanov, A. Ultrasound contrast agents: Development of the field and current status. In: Krause, W., editor. Contrast Agents II. Vol. 222 of Topics in Current Chemistry. Springer; Berlin/Heidelberg: 2002. p. 73-106.

Ku DN. Blood Flow in Arteries. Annual Review of Fluid Mechanics. 1997; 291:399–434.

Larina IV, Evers BM, Esenaliev RO. Optimal drug and gene delivery in cancer cells by ultrasound-induced cavitation. Anticancer research. 2005; 25:149–156. [PubMed: 15816532]

Li H, Fan Y, Kodzius R, Foulds IG. Fabrication of polystyrene microfluidic devices using a pulsed CO2 laser system. Microsystem Technologies. 2011; 183:373–379.

Lim AKP, Patel N, Eckersley RJ, Taylor-Robinson SD, Cosgrove DO, Blomley MJK. Evidence for spleen-specific uptake of a microbubble contrast agent: a quantitative study in healthy volunteers. Radiology. 2004; 231:785–788. [PubMed: 15118114]

Liu Y, Yan J, Prausnitz MR. Can ultrasound enable efficient intracellular uptake of molecules? a retrospective literature review and analysis. Ultrasound in medicine & biology. 2012; 38:876–888. [PubMed: 22425381]

Marmottant P, van der Meer S, Emmer M, Versluis M, de Jong N, Hilgenfeldt S, Lohse D. A model for large amplitude oscillations of coated bubbles accounting for buckling and rupture. The Journal of the Acoustical Society of America. 2005; 118:3499–3505.

Mehier-Humbert S, Bettinger T, Yan F, Guy RH. Plasma membrane poration induced by ultrasound exposure: implication for drug delivery. Journal of controlled release: official journal of the Controlled Release Society. 2005; 104:213–222. [PubMed: 15866347]

Morgan KE, Allen JS, Dayton PA, Chomas JE, Klibanov AL, Ferrara KW. Experimental and theoretical evaluation of microbubble behavior: effect of transmitted phase and bubble size. IEEE transactions on ultrasonics, ferroelectrics, and frequency control. 2000; 47:1494–1509.

Park JI, Nie Z, Kumachev A, Kumacheva E. A microfluidic route to small CO2 microbubbles with narrow size distribution. Soft Matter. 2010; 6:630.

Patil AV, Reynolds P, Hossack JA. A non-linear three-dimensional model for quantifying microbubble dynamics. The Journal of the Acoustical Society of America. 2010; 127:EL80–86. [PubMed: 20136183]

Patil AV, Rychak JJ, Allen JS, Klibanov AL, Hossack JA. Dual frequency method for simultaneous translation and real-time imaging of ultrasound contrast agents within large blood vessels. Ultrasound in medicine & biology. 2009; 35:2021–2030. [PubMed: 19828229]

Phillips LC, Dhanaliwala AH, Klibanov AL, Hossack JA, Wamhoff BR. Focused ultrasound-mediated drug delivery from microbubbles reduces drug dose necessary for therapeutic effect on neointima formation–brief report. Arteriosclerosis, Thrombosis, and Vascular Biology. 2011a; 31:2853–2855.

Phillips LC, Klibanov AL, Bowles DK, Ragosta M, Hossack JA, Wamhoff BR. Focused in vivo delivery of plasmid DNA to the porcine vascular wall via intravascular ultrasound destruction of microbubbles. Journal of Vascular Research. 2010; 47:270–274. [PubMed: 19923850]

Phillips LC, Klibanov AL, Wamhoff BR, Hossack JA. Localized ultrasound enhances delivery of rapamycin from microbubbles to prevent smooth muscle proliferation. Journal of Controlled Release: Official Journal of the Controlled Release Society. 2011b; 154:42–49. [PubMed: 21549778]

Streeter JE, Gessner R, Miles I, Dayton PA. Improving sensitivity in ultrasound molecular imaging by tailoring contrast agent size distribution: in vivo studies. Molecular imaging. 2010; 9:87–95. [PubMed: 20236606]

Stride E, Edirisinghe M. Novel preparation techniques for controlling microbubble uniformity: a comparison. Medical & Biological Engineering & Computing. 2009; 47:883–892. [PubMed: 19434435]

Talu E, Hettiarachchi K, Powell RL, Lee AP, Dayton PA, Longo ML. Maintaining monodispersity in a microbubble population formed by flow-focusing. Langmuir: The ACS Journal of Surfaces and Colloids. 2008a; 24:1745–1749. [PubMed: 18205422]

Talu E, Hettiarachchi K, Zhao S, Powell RL, Lee AP, Longo ML, Dayton PA. Tailoring the size distribution of ultrasound contrast agents: possible method for improving sensitivity in molecular imaging. Molecular Imaging. 2007; 6:384–392. [PubMed: 18053409]

Talu E, Powell RL, Longo ML, Dayton PA. Needle size and injection rate impact microbubble contrast agent population. Ultrasound in Medicine & Biology. 2008b; 34:1182–1185. [PubMed: 18295967]

Tan YC, Cristini V, Lee AP. Monodispersed microfluidic droplet generation by shear focusing microfluidic device. Sensors and Actuators B: Chemical. 2006; 114:350–356.

Tartis MS, McCallan J, Lum AFH, LaBell R, Stieger SM, Matsunaga TO, Ferrara KW. Therapeutic effects of paclitaxel-containing ultrasound contrast agents. Ultrasound in medicine & biology. 2006; 3211:1771–80. [PubMed: 17112963]

Wang S, Dhanaliwala AH, Chen JL, Hossack JA. Production rate and diameter analysis of spherical monodisperse microbubbles from two-dimensional, expanding-nozzle flow-focusing microfluidic devices. Biomicrofluidics. 2013; 71:014103.

Wible JH, Wojdyla JK, Bales GL, McMullen WN, Geiser EA, Buss DD. Inhaled gases affect the ultrasound contrast produced by albunex in anesthetized dogs. Journal of the American Society of Echocardiography: official publication of the American Society of Echocardiography. 1996; 9:442–451. [PubMed: 8827627]

Zemp RJ, Tavakkoli J, Cobbold RSC. Modeling of nonlinear ultrasound propagation in tissue from array transducers. The Journal of the Acoustical Society of America. 2003; 113:139–152. [PubMed: 12558254]

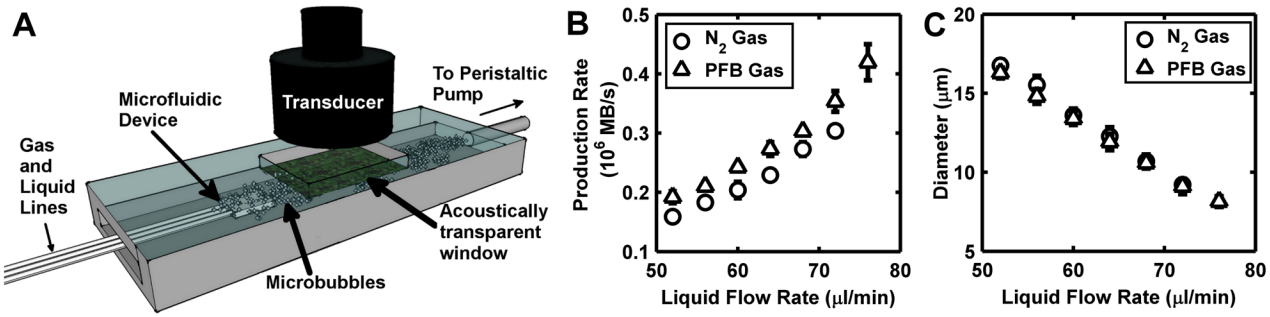

Figure 1.

(A) Schematic of the *in vitro* flow chamber. A flow-focusing microfluidic device produced microbubbles *in situ*. Calcein was administered alongside the microbubbles, and a single element ultrasound transducer insonated the microbubbles as they flowed by confluent rat aortic smooth muscle cells. Microbubble (B) production rate and (C) diameter as a function of the FFMD liquid flow rate (pressure was held constant at 55.2 kPa).

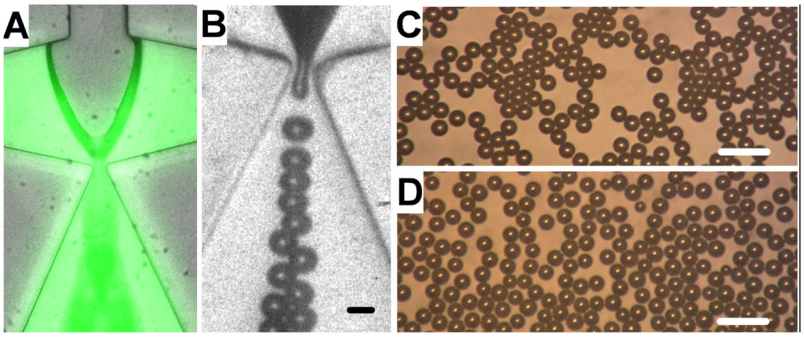

Figure 2.

(A) Image of calcein incorporated into the liquid phase of the FFMD. (B) High speed image showing PFB microbubble production (scale bar = 10 μm). (C) PFB and (D) nitrogen microbubbles observed immediately after production by the FFMD (scale bar = 40 μm).

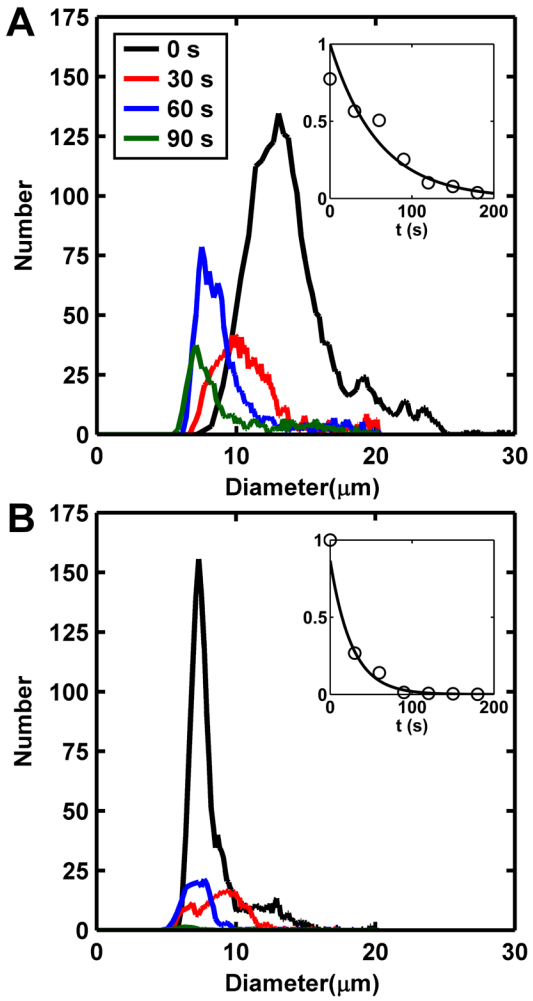

Figure 3.

Size distribution for microbubbles composed of (A) PFB and (B) nitrogen as a function of time. Microbubble diameters were measured as 8 μm within the FFMD prior to exposure to air-saturated saline. Insets: Exponential fit to microbubble counts as a function of time (R^2 = 0.95 and 0.97 respectively). The half-lives for PFB and nitrogen microbubbles were 40.7 seconds and 18.2 seconds, respectively.

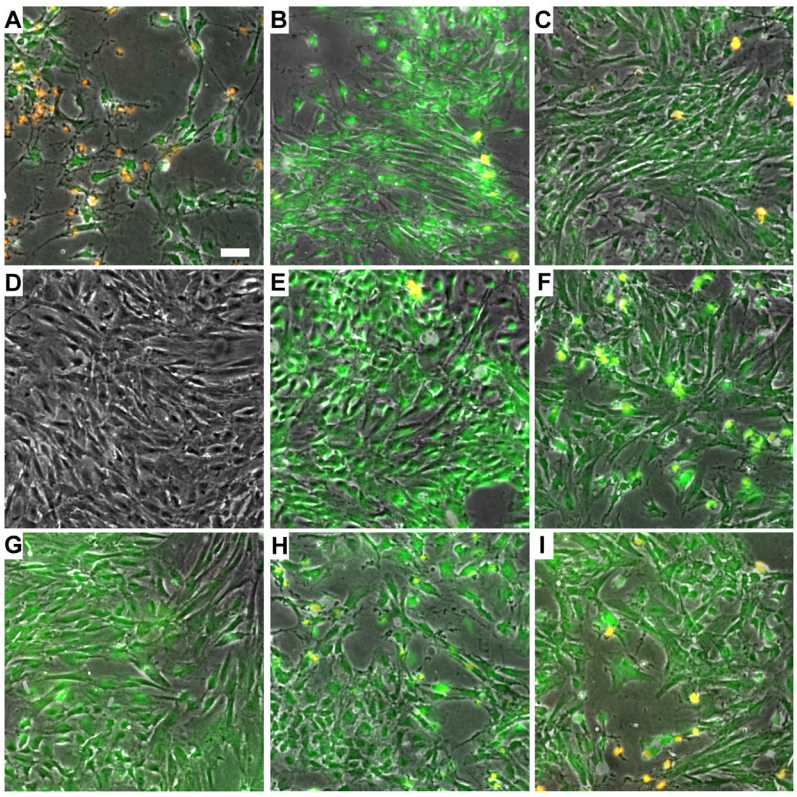

Figure 4.

Fluorescence microscopy images of rat aortic smooth muscle cells following ultrasound-mediated calcein delivery. Green fluorescence corresponds to calcein internalization while orange corresponds to cell death (scale bar = 50 μm). (A–C) Representative results of calcein delivery at 2, 9, and 18 ml/s flow rates, respectively. Ultrasound peak negative pressure was 300 kPa, and the FFMD produced 10 μm diameter PFB microbubbles at a rate of 300,000 microbubbles/s. (D–F) Calcein delivery using PFB microbubbles at ultrasound peak negative pressures of 100, 200, and 300 kPa, respectively. (G–I) Calcein delivery using nitrogen microbubbles at ultrasound peak negative pressures of 100, 200, and 300 kPa, respectively. In (D–I), the flow rate was maintained at 9 ml/s, and the FFMD produced 10 μm diameter microbubbles at a rate of 300,000 microbubbles/s.

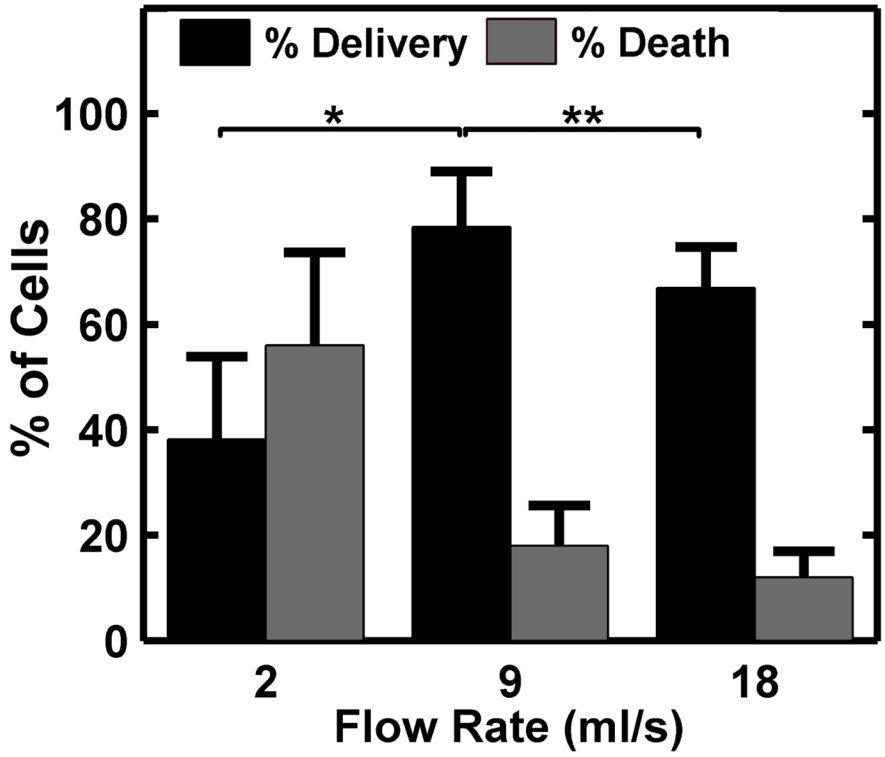

Figure 5.

Calcein delivery efficiency and percent cell death at 2, 9, and 18 ml/s flow rates. The ultrasound peak negative pressure was maintained at 300 kPa and the FFMD produced 10 μm PFB microbubbles at a rate of 300,000 microbubbles/s. (Plotted as mean + standard deviation, n > 3, * = $p < 0.01$, ** = $p < 0.05$).

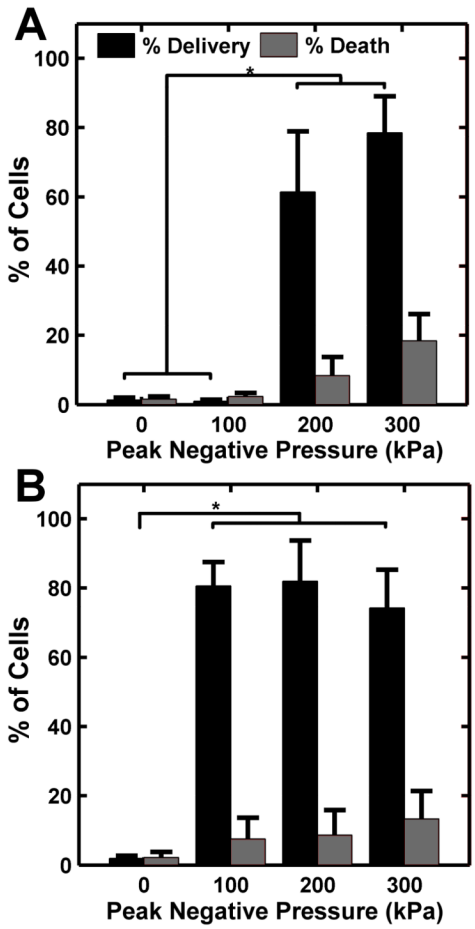

Figure 6.

Calcein delivery efficiency and percent cell death at different ultrasound peak negative pressures for microbubbles composed of (A) PFB and (B) nitrogen. Flow rate within the channel was maintained at 9 ml/s and the FFMD was set to produce 10 μm diameter microbubbles at a rate of 300,000/s. (Plotted as mean + standard deviation, n > 3, * = p < 0.01).